Carbon Vol. 28, Nos. 2/3, pp. 261–279, 1990
Printed in Great Britain.

0008-6223/90 $3.00 + .00

CARBON: AN OLD BUT NEW MATERIAL REVISITED†

P. L. WALKER, JR.
Department of Materials Science and Engineering, The Pennsylvania State University, University Park, PA 16802, U.S.A.

(*Received* 24 *July* 1989; *accepted* 8 *August* 1989)

Abstract—Three areas of our past research are considered: carbon formation from catalyzed CO decomposition over iron and from liquid phase coking of hydrocarbons, the role of carbon active sites in the C-O_2 reaction and hydrocarbon CVD processes, and production and properties of carbon molecular sieves. In each case, the importance of rate processes has been emphasized. Where possible, an attempt has been made to integrate our research findings with those of other investigators.

Key Words—Active sites, gasification, chemical vapor deposition, carbon molecular sieves, carbonization.

1. INTRODUCTION

Some of you may recognize the title which I selected for this plenary lecture. I used it in 1961 for my Sigma Xi national lecture at American universities and again in 1971 for my Skakel Award lecture[1,2]. I was fortunate to be involved in carbon research during what I think was the golden era of carbon science. It started in the late 1940s and lasted until the early 1980s. This era saw the inception of materials science, with the recognition that all materials (metals, ceramics, and polymers) have much in common. In each case, their preparation and the delineation of their structure and properties involve the use of the same scientific principles. Carbon, because of its unique properties, fully participated in this materials science revolution.

What I have chosen to do in this paper is to revisit the research in which I have been involved over the past 35 years and to select some areas which particularly interest me. I will summarize our findings in these areas and attempt to relate these findings to some of today's pertinent problems (and opportunities) in carbon science. The areas will encompass:

1. preparation of carbons via catalytic cracking of CO and coking processes,
2. carbon active sites of concern in CVD and carbon gasification, and
3. microporous carbons and carbon molecular sieves.

It occurred to me when I began to prepare this paper that I will be addressing, primarily, the importance of rate processes in three different areas. Probably, rate processes have not been sufficiently addressed to date by researchers in carbon science.

Lastly, I want to recognize the indispensable contributions which my graduate students, post-docs and faculty colleagues made to this research over the many years.

2. PREPARATION OF CARBONS

2.1 *Via CO decomposition over iron*

At the time we began this research in 1952, it was well known that CO, under certain conditions, dissociated over iron, yielding a filamentous carbon. In most cases, this reaction was an undesirable by-product realized during the progress of another process or desirable reaction. We envisioned this reaction being part of a scheme to convert one form of carbon to another more desirable form of carbon. In particular, we envisioned gasifying plentiful anthracite coal, with its attendant mineral matter, using CO_2 or steam to produce CO and H_2. In turn, the pure CO or CO/H_2 mixture would be passed over an iron catalyst to dissociate the CO and produce a filamentous carbon, free of mineral matter. Or,

$$2\,CO \xrightarrow[Fe]{} C + CO_2 \qquad (1)$$

$$CO + H_2 \xrightarrow[Fe]{} C + H_2O. \qquad (2)$$

We anticipated that the unique filamentous carbon formed would have applications as a filler in composite materials.

Equilibrium favors conversion in reactions (1) and (2) at temperatures below about 700°C. Our studies on kinetics of carbon production from CO are presented elsewhere[3]. The catalyst used was reagent grade iron powder, having an average diameter on a weight basis of ~10 μm and a surface area of 0.99 m^2/g. Prior to a run, the catalyst was heated to reaction temperature in He and then held in flowing H_2 for 1 h. All runs were conducted in a flowing gas

†Plenary Lecture, Nineteenth Biennial American Carbon Conference, June 30, 1989.

stream at 0.1 MPa total pressure. We were particularly interested in the effect of temperature and gas composition on the rate of carbon formation and the amount of carbon which could be formed before the catalyst lost its activity. Figure 1 summarizes pertinent results. At a relatively low temperature (500°C), variations in the amount of H_2 added to the CO stream had little effect on the rate of carbon deposition. Further, the catalyst remained active to enhance carbon deposition for extended periods of time. On the other hand, at a relatively high temperature (630°C), increases in H_2 content in the gas mixture had a major effect on the amount of carbon which could be formed before the catalyst was essentially deactivated. It had less effect on the initial rate of carbon formation, which in all cases was greater than that found at 500°C. The mixture containing 0.8% H_2 could produce only 0.16 g of carbon. As the amount of H_2 in the mixture was increased, the amount of carbon which could be produced prior to catalyst deactivation increased dramatically. In the mixture containing 39.8% H_2, catalyst deactivation was not evident even after production of 3.8 g of carbon, or a product having a C/Fe atomic ratio of 870. One wonders if the catalyst would have ever lost its activity. Unfortunately, the reaction had to be stopped since carbon completely filled the reactor space.

The phenomena of catalyst deactivation and the possibility of catalyst regeneration was studied further, as seen in Fig. 2. X-ray diffraction patterns of the solid, removed from the reactor following catalyst deactivation, showed strong peaks for cementite (Fe_3C) and carbon. No diffraction peaks were found for Fe_3O_4, Fe_2O_3, or α-Fe. Catalyst regeneration was attempted using H_2 under conditions given in Fig. 2. Following treatment in H_2 at previous reaction temperatures (runs 1 and 3), Fe_3C was completely converted to α-Fe as seen by X-ray diffraction. Concurrently, about 0.5 g of carbon was gasified by H_2 to methane. This weight is in considerable excess of the weight of carbidic carbon associated with Fe_3C (0.007 g), indicating that the free carbon derived from CO dissociation over iron has an unusually high reactivity to H_2. As discussed previously, free carbon gasification by H_2 is usually a very slow reaction[4]; particularly at atmospheric pressure and temperatures as low as 576°C. Treatment in H_2 resulted in catalyst reactivation, as seen in Fig. 2. Run 3 was particularly interesting. The maximum rate of carbon formation over the regenerated catalyst exceeded the maximum rate found prior to catalyst deactivation. However, recurring catalyst deactivation occurred in a much shorter time period and after less new carbon had been formed.

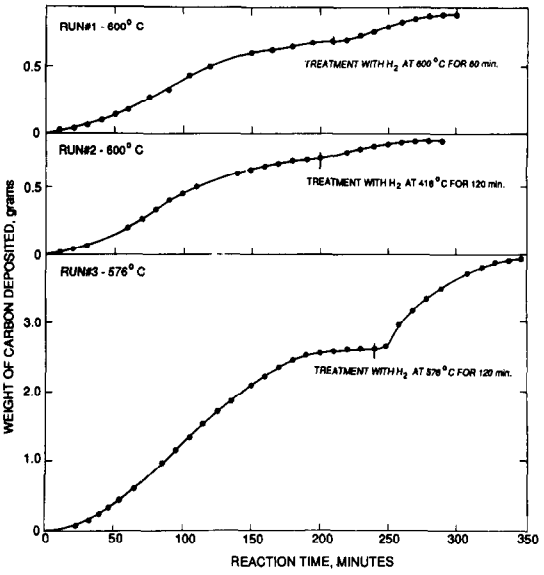

Fig. 2. Regeneration of catalyst using H_2 following carbon deposition from 99.2% CO-0.8% H_2 mixture over 0.1 g iron.

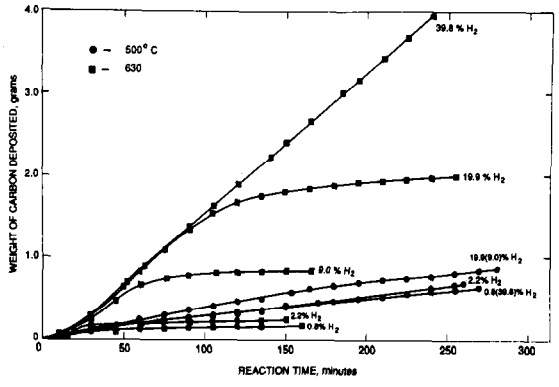

Fig. 1. Effect of CO-H_2 composition on rates of carbon deposition at 500°C and 630°C over 0.02 g iron.

Since we carried out our studies on carbon production from CO in the 1950s, much work has been done by others attempting to elucidate the mechanism of this process over an iron catalyst. It is known that CO chemisorbs on iron in the designated α_3 state, resulting in a major decrease in the strength of the carbon—oxygen bond, and in CO dissociation into carbon and oxygen atoms[5]. This is followed by dissolution of carbon atoms in the iron and bulk diffusion of carbon through the metal to the iron—carbon interface. At this location, precipitation of carbon atoms occurs, resulting in the formation of carbon filaments[6,7]. Some of the carbon atoms on the iron surface at the gas—iron interface will also combine at some rate to form a well-ordered, nonporous, lamellar carbon layer[8] which will lead to reduced access of CO to the catalyst surface, resulting ultimately in complete catalyst deactivation. It is thought that the role of H_2, as an accelerator, is to prevent the formation of this ordered carbon layer by continually gasifying the carbon atoms, producing methane, and maintaining the surface of iron in a metallic state. As expected, hydrogen also serves as an accelerator for the growth of carbon filaments in the presence of hydrocarbons[9].

The morphology of carbons produced from CO dissociation over iron has been studied by a number of workers[8,10–13]. In our studies, the most characteristic growth consisted of two carbon filaments tightly twisted into a rope over 1 μm in length and between 0.1 to 0.5 μm in diameter[14]. The length of the filaments depends upon the weight of carbon produced from a starting catalyst weight. Much bifilamentary growth also was observed, where the carbon filaments did not become twisted. In most cases, the filaments were hollow in their center. At one end of the carbon growths, there invariably was located a particle of iron and/or iron carbide. However, as has been reported many times, the process of carbon formation resulted in fragmentation of the starting iron particles (10 μm in diameter) to much smaller sizes (<0.1 μm in size). This is thought to be due to carbon formation (and consequently pressure build-up) along iron grain boundaries.

We characterized the crystallinity and surface area of the carbons formed[14]. The temperature of formation, the amount of carbon formed, and the CO/H_2 feed ratio used all affected carbon properties. Results can be briefly summarized in Table 1, on selected samples, where 0.1 g of iron was used to produce 0.9 g of carbon. As expected, the C/H atomic ratio of the carbon increased as the CO/H_2 feed ratio and formation temperature were increased. The effect of feed ratio and formation temperature on carbon crystallinity was more complex. For the feed containing 0.8% H_2, there was relatively little effect of formation temperature on carbon crystallinity. In contrast for the feed containing 39.8% H_2, carbon crystallinity increased significantly with increasing formation temperature. The lowest interlayer d-spacing found, 0.3359 nm, is indicative of a carbon having ~85% three dimensional stacking order in the c-direction, according to the Franklin correlation[15]. In any event, the carbons formed have an unusually high degree of crystallinity, considering the relatively low formation temperatures used. The surface areas of the carbons, as measured by N_2 adsorption at −196°C, generally decreased sharply with increasing formation temperature. Surface areas are unusually high considering the degree of crystallinity found for the carbons. As discussed previously[1], it means that the carbons have some of the lowest crystallite area to gas adsorption area ratios of any carbon studied.

Properties of the final carbon are strongly dependent upon the amount of carbon formed from a starting weight of iron catalyst. Table 2, for example, summarizes results for carbons produced from a 99.2% CO–0.8% H_2 mixture at 528°C over a 0.1 g of iron. The crystallinity of the carbon decreases and its surface area increases as more carbon is formed.

The graphitizability of CO carbon produced at 528°C was examined and compared with that of needle petroleum coke. Results are summarized in Table 3. The petroleum coke was considerably more graphitizable than the CO carbon. This is attributed to the excellent crystallite alignment in the 1000°C needle coke over large distances, which is consistent with its low surface area of 0.8 m^2/g. The poor graphitizability of the CO carbon suggests that it has poor crystallite alignment over large distances, which is consistent with its having a high surface area. Difficulty in the graphitization of CO carbons has been more recently noted[12]. They attribute the persistence of structural disorder upon heat treatment to high temperatures to the experimental fact that, already at 400°C, the basal planes in a catalytic carbon are relatively large in size. A higher activation energy is, therefore, necessary for ordering such large perfect layers than for ordering small units connected by low angle tilt and twist boundaries.

Recently, Dresselhaus and coworkers reported that the graphitizability of carbon fibers depends upon their diameter[16]. Thick fibers (diameter ~10 μm) produced from methane or benzene at 1100°C have a very high degree of graphitizability[7]. However, thinner fibers (diameter ~0.1 μm) show only partial graphitization[16]. They conclude, in agreement with Oberlin[17], that decreasing graphitizability for the thinner fibers is due to their having layer planes with smaller radii of curvature. For fibers of smaller diameter, they find a graphitized skin and a turbostratic core (a two-phase carbon).

It is appreciated that fibers produced from methane or benzene at 1100°C consist of two types of carbon prior to their heat treatments at elevated temperatures. The inner core is composed of the catalytic carbon which grows very rapidly in the axial direction. On to the inner core, CVD carbon grows thermally in the radial direction. The larger the diameter of the fiber, the greater will be the volume fraction of CVD carbon for a fixed size of catalyst particle. As discussed earlier, Audier *et al.*[12] con-

Table 1. Effect of $CO-H_2$ composition and formation temperature on carbon properties[14]

	0.8% H_2				39.8% H_2			
Temperature (°C)	C/H Ratio	L_c (nm)	*d*-spacing (nm)	Surface area (m^2/g)	C/H Ratio	L_c (nm)	*d*-spacing (nm)	Surface area (m^2/g)
500	21.5	9.7	0.3384	113	7.3	4.0	0.3443	152
528	25.3	12.4	0.3370	111	10.2	5.4	0.3431	156
576	27.3	12.7	0.3369	87	14.3	15.4	0.3365	105
602	—	10.1	0.3380	71	16.4	19.1	0.3360	65
630	34.2	11.4	0.3374	35	—	28.0	0.3359	89

Table 2. Changes in properties of carbons with amount formed from a 99.2% CO-0.8% H_2 mixture at 528°C[14]

Carbon formed, (g)	L_c (nm)	*d*-spacing (nm)	Surface area (m^2/g)
0.09	14.5	0.3365	83
0.92	12.4	0.3370	111
2.05	11.0	0.3374	117
3.39	9.4	0.3383	131
4.63	9.7	0.3384	143
6.87	8.7	0.3384	144

clude that catalytic carbon formed at low temperatures is not particularly graphitizable. On the other hand, carbon containing small units connected by low angle tilt and twist boundaries (which may describe the CVD carbon) could be much more graphitizable. This, then, is a possible alternate explanation for the effect of carbon fiber diameter on graphitizability.

The CO carbon fibers which we have been discussing, formed at temperatures between 500–630°C, were clearly composed almost entirely of catalytic carbon. At these temperatures chemisorption and dissociation of CO over carbon active sites to form CVD carbon would be a very slow process[18]. The poor graphitizability of the CO carbon fibers may be due to the overwhelming presence of catalytic carbon and/or the fact that the fibers were of small diameter.

2.2 *Via carbonization in the liquid phase*

The carbonization of organic precursors in the liquid phase at temperatures between about 400–550°C is the most important process (certainly tonnage-wise) for the production of carbons. It encompasses, for example, the production of metallurgical cokes from caking coals, petroleum cokes from petroleum feed stocks, and fibers from petroleum and coal tar pitches. Consequently, large amounts of research have been conducted on understanding the carbonization process. In the author's judgement, the most important discovery in the carbonization process can be attributed to Brooks and Taylor[19,20]. In 1964, they discovered that the formation of graphitizing low-temperature cokes by solidification from a liquid phase proceeds via the separation of a mesophase (or intermediate phase) having properties similar to those of liquid crystals. The nature of the mesophase is dependent upon

1. the extent of planarity of intermediate compounds formed,
2. rates of carbonization,
3. fluidity and extent (duration) of fluidity of liquid phase, and
4. the possible effect of solids on mesophase formation and coalescence.

We will consider some of the research done in our laboratory intended to elucidate the importance of items (1) and (2) in the carbonization process.

2.2.1 *Carbonization of individual organic compounds.* Coal and petroleum feedstocks, which are used to produce cokes and graphites via liquid phase carbonization, are composed of many organic compounds of varying structures, molecular weights, and heteroatom contents. Elucidating the fundamentals of carbonization, by using these feedstocks as precursors, is thus made most difficult. Therefore, workers in a number of laboratories have chosen to study the carbonization of individual organic compounds which are important constituents of commercial feedstocks[21–40].

Of particular interest for study as precursors are planar, polyaromatic hydrocarbons (PAH) since they frequently lead to a Brooks and Taylor liquid crystal mesophase upon carbonization and ultimately to graphitizable carbons. The chemistry of carbonization of these compounds involves at least the following important processes:

1. disproportionation of two PAH molecules into one free radical molecule and one hydroaromatic molecule,
2. condensation (polymerization) of free radicals into larger molecular weight aromatics, and
3. cleavage of hydroaromatic molecules giving smaller liquid and gas-phase species.

Understanding the detailed chemistry of carbonization of even a single aromatic hydrocarbon can be extremely complicated, as discussed by Stein[41]. Rather than focus on the details of this chemistry, we chose to focus on the effect of the structure of aromatic compounds and their carbonization rates on the graphitizability of cokes ultimately produced. Carbonization was conducted in batch reactors under either autogenous pressure or an inert gas pressure. The progress of carbonization was monitored by measuring the formation of pyridine insolubles as a function of reaction temperature and time under essentially isothermal conditions[26,35,37,40].

Consider our studies on the isomers anthracene (I), a linear aromatic, and phenanthrene (II), a branched aromatic, shown in Fig. 3. They have molecular weights of 178 and are completely soluble in pyridine. Upon their carbonization, the disappearance of pyridine solubles with time exhibits first order kinetics over large ranges of conversion, allowing

Table 3. Graphitizability of CO carbon and needle petroleum coke[14]

Sample	Temperature (°C)	L_c (nm)	*d*-spacing (nm)
CO carbon	528	14.4	0.3373
CO carbon	2500	21.7	0.3373
CO carbon	3000	26.9	0.3371
Petroleum coke	~1000	3.4	0.3482
Petroleum coke	3000	84.0	0.3362

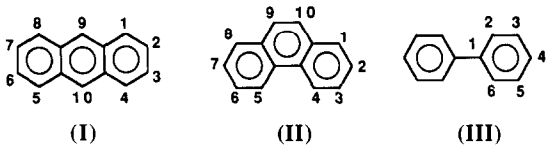

Fig. 3. Molecular structures of anthracene (I), phenanthrene (II), and biphenyl (III).

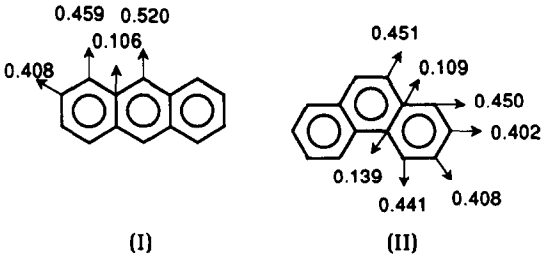

Fig. 5. Free valence indices at different positions in the anthracene and phenanthrene molecules.

the calculation of a rate constant. Values of the rate constants are summarized on Arrhenius plots, Fig. 4. In the temperature range where carbonization proceeds at a significant rate (to be of commercial interest) and still occurs in the liquid phase (below critical temperatures), anthracene carbonizes much more rapidly than does phenanthrene. This has been known at least since the pioneering studies of Madison and Roberts[22]. Under our conditions, rate constants for the carbonization of anthracene and phenanthrene are given by $1.4 \times 10^{13} \exp(-192\ \text{kJ/mole/RT})\ h^{-1}$ and $3.5 \times 10^{20} \exp(-313\ \text{kJ/mole/RT})\ h^{-1}$, respectively[35,37].

Attempts have been made to correlate the thermal reactivities of PAH with reactivity indices derived from molecular orbital theory[23,42,43]. Molecular orbital theory shows that the total bond orders and, hence, free valence indices of carbon atoms vary with their location in the PAH. Further, it has been shown that reactivities of particular carbon atoms increase as their free valence indices increase. Figure 5 presents values of free valence indices at particular locations in the anthracene and phenanthrene molecules[42,44]. These data make two important points. First, the free valence index at the central carbon atoms (the 9 and 10-positions) in anthracene is by far the highest of any position in either molecule. Thus, this position is expected to have the highest reactivity for the loss of hydrogen and formation of a free radical. This is consistent with anthracene showing a much higher reactivity for carbonization than does phenanthrene. Second, the spread of free valence indices in anthracene is much greater than in phenanthrene. This means that reactivities at different carbon sites in anthracene are expected to show a greater spread than in phenanthrene. Consider the implication of these differences in reactivity within a PAH on the quality of mesophase and then semi-coke which can be formed upon carbonization.

Because of the high reactivity at the 9-position, carbonization of anthracene leads first to predominantly 9–9′ bianthryl (IV), followed by the formation of dibenzoperylene (V), and bianthene (VI). That is,

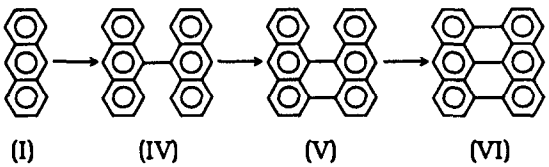

(3)

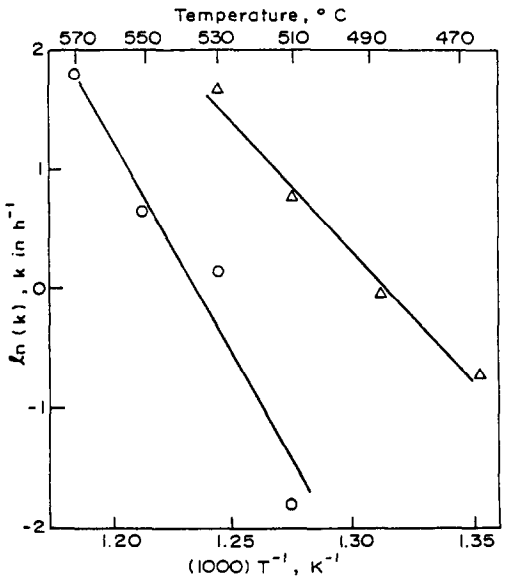

Fig. 4. Arrhenius plots for the formation of pyridine insolubles from the carbonization of (△) anthracene[35] and (○) phenanthrene[37].

As indicated by Lewis[33], dehydrogenation of bisanthene can lead to further condensation polymerization. The result is the formation of large, planar, fully condensed PAH molecules which are expected to align parallel, due to dispersion forces, to form anisotropic liquid crystal domains when dispersed in a fluid isotropic medium. Lewis notes that eleven dimeric structures can be formed from anthracene but that most of them do not possess the right steric conformation to undergo an additional dehydrogenation reaction to give a fully condensed (and planar) molecule containing only six-membered rings[34,36]. Thus, the importance of the high reactivity at the 9 and 10-positions in anthracene, relative to reactivities at the other positions, is obvious in determining the predominant and desirable reaction pathway during carbonization.

If upon carbonization the phenanthrene molecule undergoes dehydrogenation at its most reactive 9 (and 10) and 1 (and 8) positions to form free radicals, polymerization reactions can eventually lead to the planar structure, shown in Fig. 6. This structure and higher molecule weight species produced from it

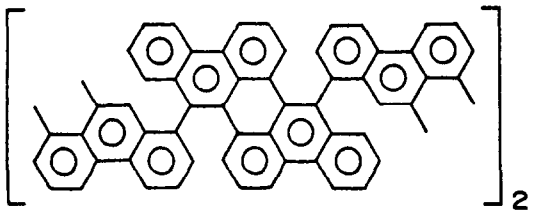

Fig. 6. Structure formed by fusing the 9 and 1 positions of phenanthrene together following production of free radicals by dehydrogenation.

would be expected to be precursors of graphitizable carbons. The problem is that since the free valence indices at the 1 and 4 positions in phenanthrene are essentially equal to the index at the 9 position, free radical formation at these sites is expected to occur at an important rate. Condensation polymerization at these positions will not lead to fully condensed, planar molecules. To the extent that dehydrogenation and free radical formation were to occur at the 2 and 3 positions, leading to the formation of biphenanthryls, Fig. 7, the development of anisotropic domains in the mesophase would also be drastically reduced. These dimers could not undergo further intramolecular condensation reactions. Also, we will see in a moment the retarding effect which the introduction of a molecule (biphenyl) exhibiting free rotation about the single bond forming the two monomers (as do the biphenanthryls) can have on the production of a graphitizable semi-coke.

Experimental results confirm that anthracene leads to the production of a coke which is more graphitizable than phenanthrene and that its graphitized carbon contains a greater crystallite alignment[26]. Results are summarized in Table 4 for cokes produced at 550°C.

The carbonization temperature used would also be expected to have an effect on the graphitizability of the semi-coke produced since it will change the span of rates at which free radicals are produced at different carbon sites in PAH. As the carbonization temperature of phenanthrene is increased, the production of free radicals at the 2, 3, and 4 positions, relative to the 1 and 9 positions, is expected to increase since dehydrogenation of these positions is expected to require higher activation energies. As just discussed, this should mean that more undesirable reactions will occur during carbonization of phenanthrene, leading to the production of a less graphitizable coke. Studies by Peters in our laboratory[37] confirm this reasoning, as shown in Table 5. In each case the semi-coke used for calcining and graphitization studies contained about 90% pyridine insolubles.

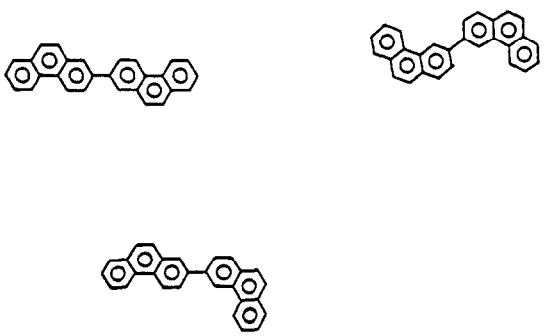

Fig. 7. Formation of nongraphitizable biphenanthryls through reactions at the 2 and 3-positions in phenanthrene.

Table 4. X-ray diffraction measurements on carbons produced at 2800°C from different cokes[26]

Precursor	*d*-spacing (nm)	L_c (nm)	Relative Intensity of (002) Peak
Anthracene	0.33618	>100	100
Phenanthrene	0.33680	99	73
Biphenyl	0.346	3.5	13

2.2.2 *Carbonization of binary mixtures of organic compounds.* Two binary systems were selected for carbonization and graphitization studies: anthracene—biphenyl and phenanthrene—biphenyl[26,28]. Biphenyl (III) was selected for the second component in the binary mixtures for two reasons. First, the carbonization of biphenyl leads to randomly structured aromatic polymers which are nongraphitizable[33]. It was of interest to observe the possible retardation of the graphitizability of cokes produced from anthracene and phenanthrene by its introduction. Second, Tilicheev reported that the thermal reactivity of biphenyl is close to that of phenanthrene, while being three-orders of magnitude less reactive than anthracene at 450°C[45]. Therefore, these binary mixtures gave us the possibility of studying the effect which similar and diverse reactions rates have on their carbonization processes. Carbonizations were carried out under N_2 at pressures ranging between 7.3–9.8 MPa at 550°C.

For the anthracene—biphenyl system, cokes of inhomogeneous texture were produced, some regions exhibiting anisotropic character (similar to that derived from pure anthracene), other regions exhibiting isotropic character (similar to that derived from pure biphenyl). In contrast, cokes produced from the phenanthrene—biphenyl system exhibited a much greater homogeneous texture, with the size of anisotropic regions decreasing sharply upon small additions of biphenyl. Table 6 presents X-ray diffraction results on the carbons produced upon heat treatment of the cokes to 2800°C. The (002) X-ray diffraction peaks from carbons produced from anthracene-biphenyl mixtures exhibited a sharp peak, clearly derived from the anthracene-carbon, superimposed on a broad peak derived from the biphenyl carbon. X-ray diffraction results for the sharp peak are given in Table 6. A two-phase carbon existed where biphenyl had a negligible effect on the nature of the carbon derived from the anthracene precur-

Table 5. X-ray diffraction studies on carbons produced at 2500°C from phenanthrene cokes[37]

Carbonization temperature (°C)	*d*-spacing (nm)	L_c (nm)	L_a (nm)	Relative intensity of (002) peak
510	0.3363	130	106	100
550	0.3366	113	79	31
570	0.3373	83	50	23

sor. By contrast, the (002) X-ray diffraction peaks for carbons produced from phenanthrene—biphenyl mixtures exhibited just one peak, which progressively became broader and weaker as more biphenyl was introduced into the original mixture. These results are interpreted on the basis of reactivities of the individual hydrocarbons. Since anthracene has a much, much higher reactivity than does biphenyl, its carbonization was essentially completed before that of biphenyl commenced. Thus, free radicals produced during biphenyl carbonization interacted to a negligible extent with those produced during anthracene carbonization. Insignificant amounts of mesophase exhibiting nonplanar structures, derived from anthracene, were produced. In contrast, phenanthrene and biphenyl carbonized at similar rates. Free radicals produced during biphenyl carbonization effectively interacted with those produced during phenanthrene carbonization, leading to cross-linked, nonplanar mesophase structures (polymers). As the amount of biphenyl in the mixture was increased, biphenyl radicals reacted with an increasing fraction of the phenanthrene radicals produced upon carbonization, leading to cokes of progressively poorer graphitizability.

A number of workers have recognized the importance of reactivity and coking rates while studying the carbonization of important petroleum and coal feedstocks. Mochida and coworkers note that the carbonization reaction proceeds through radical initiation, propagation, recombination (condensation), and termination[46]. They conclude that at too high a carbonization temperature, all of these processes take place too rapidly; and there is little time for growth of an isochromatic area prior to fluidity of the medium decreasing to too low a level. As we have seen, carbonization reactivity is related to structural indices. The reactivity of aromatics is also markedly affected by the presence of alkyl chains[39], C—O bonds[46], and nitrogen within the aromatic rings[40].

Some years ago White and Price found it convenient to divide the precursor components in refinery feedstocks into two groups:

1. fast-reacting components which precipitate fine spherules at relatively low temperatures upon carbonization and
2. slow-reacting components which precipitate mesophase spherules at higher temperatures[47].

The fast-reacting components are usually associated with the asphaltene fraction of the feed and contain an abundance of oxygen functional groups. Eser *et al.*[48] took advantage of differences in reactivity of the components in petroleum residua to improve coke texture derived upon carbonization. They showed that thermal pretreatment at temperatures between 350–400°C essentially completed the carbonization of the very reactive (undesirable) precursors. If then this was followed by carbonization of the main fraction of the feed at 450°C, the extent of development of large, isochromatic regions was markedly enhanced as was graphitizability of the coke produced. It is somewhat reminiscent of results for the anthracene—biphenyl system where carbonization of biphenyl did not interfere with carbonization of anthracene.

Table 6. X-ray diffraction measurements on carbons produced at 2800°C from different cokes[26,28]

Precursor composition	*d*-spacing (nm)	L_c (nm)	Relative intensity of (002) peak
Anthracene—biphenyl			
100% (I)	0.33618	>100	100
75% (I)–25% (III)	0.33605	>100	99
50% (I)–50% (III)	0.33655	>100	98
100% (III)	0.346	3.5	13
Phenanthrene—biphenyl			
100% (II)	0.33680	99	73
95% (II)–5% (III)	0.33718	49	—
90% (II)–10% (III)	0.33743	43	60
75% (II)–25% (III)	0.33882	22	39
50% (II)–50% (III)	0.3425	7.1	21
100% (III)	0.346	3.5	13

In conclusion to this section it seems apropos to quote Lewis[36]. "It is thus clear that the thermal polymerization process (carbonization) leads to a mixture of molecules (some of) which have the appropriate sizes and shapes to undergo association and ordering to form a nematic liquid crystalline phase. The extent of (anisotropic) mesophase development is related to both the chemical structure and the concentration of these various components."

3. IMPORTANCE OF ACTIVE SITES TO CARBON SCIENCE

Graphite crystals exhibit properties which are highly anisotropic, due to weak van der Waals bonding between basal planes (in the *c*-direction) and strong covalent bonding within basal planes (in the *a* and *b* directions). As expected, graphite crystals exhibit large differences in surface energies in their different crystallographic directions[49]: about 0.11 J/m^2 in the basal plane and 5 J/m^2 in the prismatic planes. It would be expected that large differences would exist in the rates of interaction of gases and vapors when exposed to the basal plane surface as compared to the edge or prismatic surfaces. The edge surface would be found at the termination of the carbon (trigonally bonded) basal planes, as well as at defects (vacancies, dislocations, and steps) located within the basal plane. The edge surface would be expected to react much more rapidly with gases and vapors than does the basal plane surface. Thus it will be given the name, active surface.

The extent to which each carbon contains active area is of overwhelming importance as to how that carbon will behave under different situations such as its exposure to oxidizing gases (adsorption and carbon gasification), exposure to hydrocarbons (adsorption and chemical vapor deposition processes), and exposure to a binder phase (matrix) in the preparation of carbon composites. We will consider the importance of active surface area (ASA) in the first two items listed above in the following sections.

3.1 *Specific reactions rates for the C-O_2 reaction*

We will first consider how studies on the gasification of carbons of very large crystallite size and excellent crystallite alignment in O_2 have enabled the obtaining of meaningful specific reaction rates. In essence, the use of electron or light microscopy (or in selected cases, just the eye) will enable us to identify the ASA in these carbons; and by following the recession of this ASA as a function of time as carbon gasification in O_2 proceeds, kinetic data will be obtained. We will later consider studies on the gasification of polycrystalline carbons of much smaller crystallite size and much poorer crystallite alignment where other techniques must be used to identify their ASA. We will see that these latter techniques can offer some problems in obtaining a quantitative measure of ASA.

3.1.1 *From measuring recession rates of active sites.* Hennig pioneered the use of electron microscopy to follow the enlargement of vacancies in the presence of O_2 as a function of time and thereby determine gasification rates at active sites[50]. Hennig named this approach the etch-decoration technique:

1. etching in O_2 which attacks the edges of vacancies one basal plane deep and thereby enlarging them and
2. decorating them by evaporating gold onto the basal plane at ~250°C.

Figure 8 shows the result of such an approach, looking down on the basal plane of a highly purified natural graphite crystal. Hennig found that the rate of increase in loop diameter was independent of loop diameter over a wide range.

Table 7 summarizes conditions used by all workers in obtaining specific reaction rates, described in this section. Figure 9, an Arrhenius plot, gives the results of Hennig (among other workers) for an O_2 pressure of 1.3 kPa. The rate of enlargement of the vacancies is given in units of cm/s. This rate can be converted into other useful specific reaction rates from a knowledge that:

1. the true density of graphite is 2.268 g/cm^3, leading to units of atoms C gasified/cm^2 ASA/s and
2. a carbon atom in the active surface occupies ~0.083 nm^2, leading to units of atoms C gasified/atoms C available for reaction in the ASA/s (which is commonly called a turn-over number (TON) in units of 1/s).

Other workers, including J. J. Baker[51], Evans *et al.*[52] and Yang *et al.*[53], used the etch decoration technique to measure the rate of expansion of vacancies in O_2 using natural graphite crystals. Their results are also summarized in Fig. 9. Results in all cases have been normalized to an O_2 pressure of 1.3 kPa (the pressure Hennig used) assuming rates are proportional to $p_{O_2}^{0.5}$.

R. T. K. Baker and coworkers[54,55] pioneered the use of in-situ controlled atmosphere electron microscopy (CAEM) to study the enlargement of multilayer channels in natural graphite crystals in the presence of O_2. The channels had been produced by previous gasification in the presence of metal catalyst particles. Their kinetic results are also summarized in Fig. 9.

Thomas and coworkers pioneered the use of light microscopy to measure recession rates of multilayer steps and other defects in the basal plane of natural graphite crystals in the presence of O_2[56]. Results are summarized in Fig. 9. Thomas and coworkers note[57] that gasification rates which they measured at single steps are considerably smaller than those which they measured at multistep defects. They suggest reasons for this possible difference, but their consideration should await the production of more

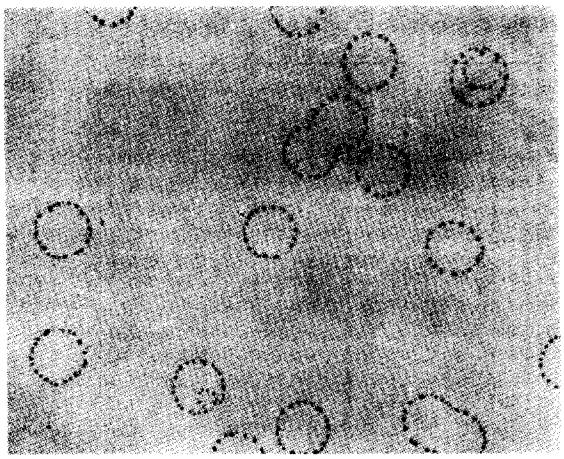

Fig. 8. Loops in the top (mostly) basal plane of natural graphite produced by carbon gasification in O_2 at vacancies[50].

evidence on the subject since results of Hennig (attack at single steps) and R. T. Baker *et al.* (attack at multisteps) are in close agreement (Fig. 9).

This laboratory pioneered the use of stress recrystallized pyrolytic graphite (SRPG) to measure specific reactions rates for the C-O_2 reaction. Figure 10 shows a piece of SRPG. Figure 11 is a light micrograph of the basal plane following an O_2 etch to 1% burn-off at 750°C. Crystallite boundaries and defects within the basal planes of crystallites are preferentially etched and, thus, demarcated. SRPG's have crystallite sizes >1 μm and a very high degree of crystallite alignment[58,59]. Specific reaction rates for carbon gasification can be easily obtained by following recession of the edge surface as a function of time using a micrometer. Recession rates are constant over large extents of burn-off[60]. Results of Rodriquez-Reinoso and Walker are shown in Figure 9. The specific reaction rate for this multilayer recession agrees more closely with values of Hennig[50] and J. J. Baker[51], obtained from single layer recession, than with the Thomas values[56], obtained from multilayer recession. This again places into doubt the conclusion of Thomas and coworkers that ASA composed of multilayers is more reactive than ASA composed of single layers.

3.1.2 *From measuring ASA using physical and chemical adsorption.* For carbons of small crystallite size and poor crystallite alignment or carbons of relatively larger crystallite size which have undergone a high degree of communition, it is not possible to follow, visually, recession of the ASA during gasification. This laboratory pioneered the use of oxygen chemisorption on these carbons at low temperatures, in the absence of carbon gasification, in an attempt to measure quantitatively the ASA which would take part in carbon gasification at higher temperatures. The rationale for the approach was that overall carbon gasification by O_2 can be divided into two steps. First is an adsorption step,

$$2\,C_f + O_2\,(g) \longrightarrow 2\,C(O), \qquad (4)$$

where two carbon free sites, 2 C_f, form an activated complex with molecular oxygen leading to its dissociation to produce, in this case, two surface carbonyl groups. This is followed by a desorption step,

$$2\,C(O) \longrightarrow 2\,CO\,(g). \qquad (5)$$

We have studied the kinetics of oxygen chemisorption on carbons exhaustively and shown that *clean* carbon surfaces possess some very active sites on which dissociative chemisorption can be followed at temperatures at least as low as −78°C[61]. From rate measurements we have identified chemisorption on five types of sites between −78°C and 160°C, with the activation energy for adsorption increasing incrementally from 13 kJ/mole on the most active sites to 52 kJ/mole on the least active sites. That the basal plane of carbon is terminated by a number of configurations of carbon atoms is expected, as depicted by Smith[62], and shown in Fig. 12. Our original thought that dissociative chemisorption of molecular oxygen would only occur in significant amounts on prismatic surfaces at edges of basal planes and defect sites in the basal plane has been confirmed by a number of workers[63,64]. They found negligible chemisorption of oxygen from O_2 on the basal

Table 7. Investigators obtaining specific reaction rates for the C-O_2 reaction using different approaches

Investigators	Po_2(kPa)	Carbon used	Approach
Hennig[50]	1.3	natural graphite flakes (NGF)	vacancy enlargement (VE)
J. J. Baker[51]	6.6	NGF	VE
Evans, *et al.*[52]	1.3	NGF	VE
Yang, *et al.*[53]	20	NGF	VE
R. T. K. Baker, *et al.*[54]	2.6	NGF	channel expansion (CE)
R. T. K. Baker, *et al.*[55]	0.7	NGF	CE
Thomas[56]	1.3	NGF	step recession
Rodriquez-Reinoso, *et al.*[60]	3.9	SRPG	edge recession
Laine, *et al.*[72]	5.0×10^{-3}	Graphon	appearance of CO + CO_2 plus oxygen chemisorption (a)
Taylor[73]	20	V3G	(a)
Ranish[79]	100–5100	SP-1	(a)

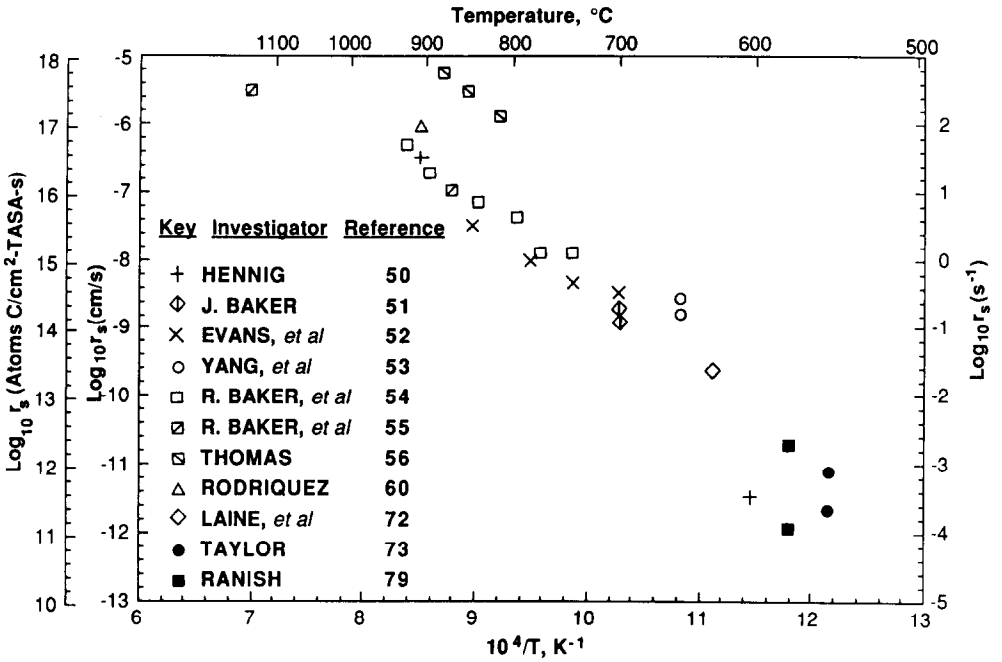

Fig. 9. Compilation of results for specific reaction rates for the C-O_2 reaction at 1.3 kPa pressure.

plane of single crystal flakes of natural graphite up to at least 400°C.

We have also studied at length the kinetics of desorption of oxygen complexes from carbons[65–68]. Pertinent facts can be summarized as follows:

1. Reaction (4) is not reversible; when desorbing chemisorbed oxygen from the carbon surface, it comes off as CO and CO_2, not O_2.

2. Essentially, consistent with the definition of chemisorption, the rate of removal of stable oxygen complexes from the carbon surface is slower than the rate of their formation. For example, oxygen chemisorbed on activated graphitized carbon black at 100°C only begins being desorbed as CO and CO_2 at ~200°C, with desorption continuing up to at least 950°C[65].

3. As expected, the activation energies for desorption of the stable oxygen complex are greater than those for adsorption. For example, oxygen chemisorbed on activated graphitized carbon black at 25°C during a 2 hr period was removed by linear thermal programmed desorption (LTPD) at temperatures between 300–1200°C, exhibiting an activation energy distribution function ranging from ~200–360 kJ/mole[68].

4. Isotopic studies indicate that oxygen complexes on carbon are more or less mobile depending upon the sites on which chemisorption occurs[65]. For example, at 250°C some O^{16} complex was first added to the carbon followed by the addition of some O^{18} complex. Upon desorbing the complex in temperature steps up to 900°C, the ratio of O^{16} to O^{18} in product CO and CO_2 was the same at each desorption temperature. In other words, the last ox-

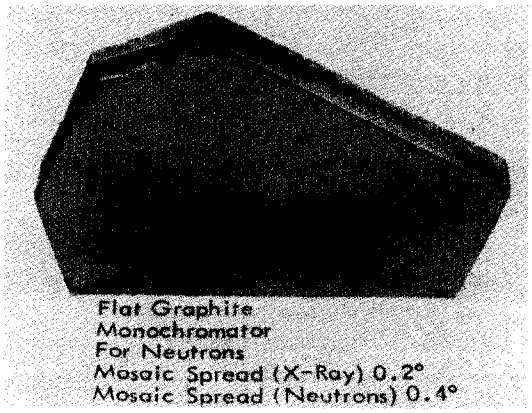

Fig. 10. Photograph of stress recrystallized pyrolytic graphite[58].

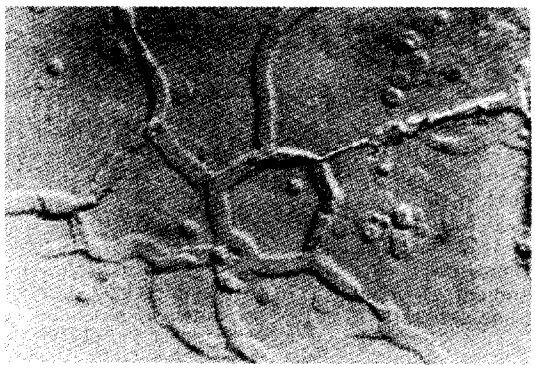

Fig. 11. Micrograph of basal surface of SRPG following O_2 etch to 1% carbon burn-off at 750°C.

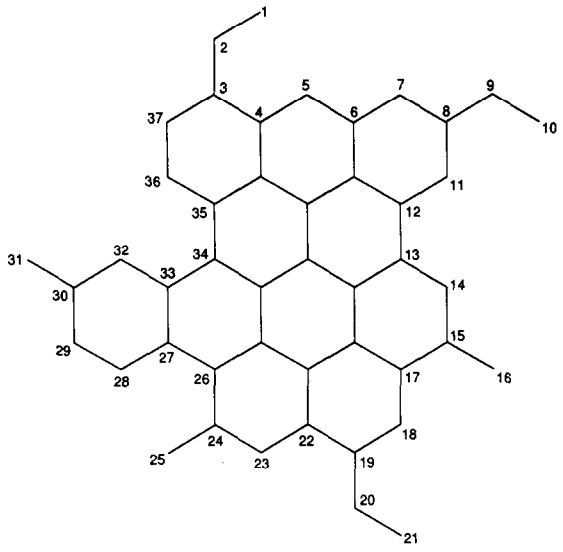

Fig. 12. A schematic arrangement of carbon atoms in a layer plane showing a variety of peripheral carbon fragments and ring positions available for attack by oxidizing gases[62].

ygen on was not the first to be desorbed, as would be expected if the oxygen complex was immobile and apriori heterogeneity of the carbon sites existed.

5. A desorption event leaves behind a new surface carbon site which is superactive, a nascent site, until it rehybridizes into a less active site. If before rehybridization is complete collision of a gas phase species with the site occurs, the probability of reaction with the site is enhanced. For example, if decomposition of an oxygen complex yielding CO occurs during a LTPD in the presence of CO_2, the rate of gasification of the carbon by the CO_2 is markedly enhanced[66,67]. Also, the rate and amount of oxygen chemisorption is increased if it is conducted at temperatures where carbon gasification is just beginning to occur at a measurable rate[65,69].

In 1959, when we started our attempt to obtain meaningful specific reactions rates for polycrystalline carbons, we were aware of some of the above facts related to reactions (4) and (5) but not all of them. Our thought was that we could find a temperature low enough to carry out reaction (4) in the absence of carbon gasification but at the same time high enough to be able to cover all the ASA with an oxygen complex within some reasonable reaction time. Then assuming that the ASA was located, primarily, in prismatic zig-zag[100] and arm-chair[110] surfaces where a carbon atom occupies on average ~0.083 nm^2 and that most of the oxygen atoms were bonded to only one carbon atom in these surfaces (a carbonyl group), the amount of oxygen complex formed could be converted to ASA.

Following up on the original suggestion of Kmetko[70], it was known by 1959[71] that when spherical carbon black particles are heated to high temperatures, they polygonize with the faces of the polyhedra consisting of basal planes, as depicted in Fig. 13. These small particles not only present a high, absolute, specific basal plane area but the fraction of their total area which is basal plane area was found to be very high[71]. Upon gasification of these particles in O_2, the fractional increase in ASA would be expected to be much higher than the fractional increase in total surface area (TSA). Thus they would be ideal for use in separating the importance of ASA from that of TSA on the kinetics of the C-O_2 reaction. As seen in Fig. 14, our studies confirmed this hypothesis when Graphon (a graphitized carbon black) was gasified in O_2 at 625°C to seven levels of burn-off up to 35%[72]. The ASA's were measured by exposing the burn-off samples to an O_2 pressure of 90 Pa for 24 h at 300°C. Under these conditions, no further oxygen uptake could be detected. On the original Graphon, the measured ASA constituted 0.29% of the TSA or ~0.2 m^2/g. Upon oxidation to 35% burn-off, the ASA increased sharply to 3.1% of the TSA, amounting to almost 4 m^2/g. The ASA increased about eighteen fold upon oxidation of the Graphon to 35% burn-off whereas the TSA increased less than two fold.

Rates of the C-O_2 reaction were then measured on each of the carbons having a different level of burn-off (or ASA) using a starting oxygen pressure of ~5 Pa in a static reactor. Using a low O_2 pressure and a mass spectrometer to follow the disappearance of O_2 and appearance of CO, CO_2, and C(O) as a function of time allowed us to obtain meaningful kinetic data at very low levels of additional burn-off beyond that which the starting samples have previously undergone. For all runs, C(O) at the completion of the runs had built up to occupy only some fraction of the ASA's previously measured, as we had expected. Rates, normalized to a basis of TSA, increased by a factor of five for the burn-off range

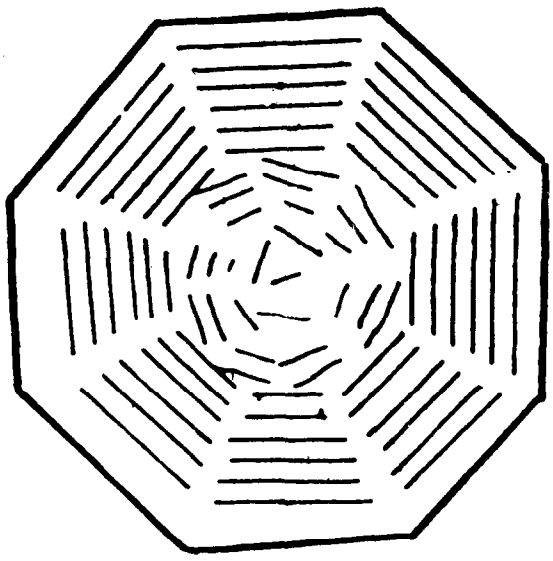

Fig. 13. Morphology of a graphitized carbon black particle.

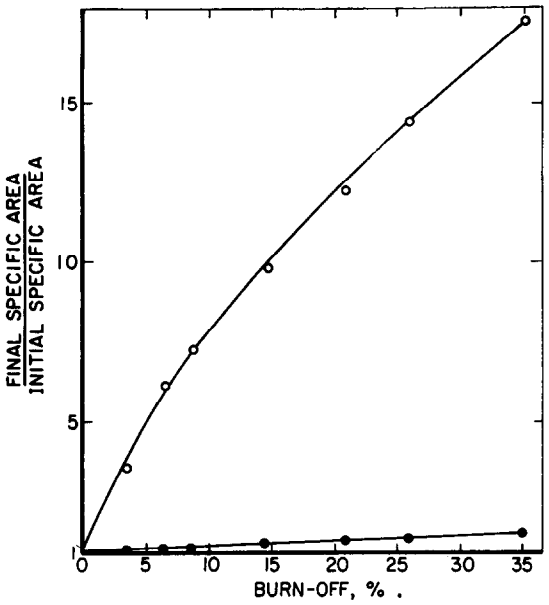

Fig. 14. Proportional increase in TSA (●) and ASA (○) with amount of burn-off of Graphon in O_2 at 625°C[72].

for the samples used. Obviously, TSA was not the concentration term determining gasification rates. By comparison, rates, normalized to a basis of ASA, were essentially constant for all burn-off samples. The specific reaction rate for Graphon, based on these studies, is shown in Fig. 9. As is seen, the value extends to a lower temperature, reasonably well, most of the specific reaction rates determined on highly crystalline graphite.

Some twenty years later Taylor, in this laboratory, studied the reactivty of graphitized carbon black in a flow reactor at 550°C with an O_2 pressure of 2×10^4 Pa[73]. This was a much higher reaction pressure than used by Laine *et al.*[72]. He used V3G, a carbon black treated to 3000°C, and quite similar to Graphon. Using a similar approach to Laine *et al.*[72], Taylor, after following reaction at 550°C to 20% burn-off, degassed the carbon at 950°C, prior to exposing it to ~90 Pa of O_2 at 300°C for 24 h. The oxygen chemisorbed was converted to an ASA of 3.0 m^2/g, in close agreement to an ASA of 2.6 m^2/g measured by Laine *et al.* following 20% burn-off of Graphon at 625°C using an O_2 pressure of 5 Pa. The problem is that the amount of oxygen recovered as CO and CO_2 upon degassing the V3G following 20% burn-off at 550°C in 2×10^4 Pa O_2 converted into a surface area of 10.5 m^2/g. That is, it markedly exceeded the ASA estimated by oxygen chemisorption at 300°C in the absence of concurrent gasification. The TSA following 20% burn-off, measured by physical adsorption of N_2 at −196°C equaled 86 m^2/g.

The question then exists as to what the proper ASA of the 20% burn-off V3G was. The question is further raised as to why the surface area covered by oxygen upon completion of 20% burn-off sharply exceeded that covered upon chemisorption at 300°C. There are at least several possible answers. First, oxygen chemisorption at lower temperatures is not successful at covering all the ASA. Some sites, where the activation energy required for oxygen dissociative chemisorption is too high, are not covered. Second, at higher gasification temperatures the mobility of some surface oxygen atoms is sufficiently high on the prismatic surfaces that it can migrate to, spill over on, and chemisorb on basal plane surfaces. A number of workers conclude that oxygen atoms can chemisorb on the basal plane composed of trigonally bonded carbon atoms[74–76].

This raises the possibility of using physical adsorption at very low pressures to determine, quantitatively, ASA. On a completely homogeneous surface, the adsorption isotherm at low pressures is linear (obeying Henry's Law) and shows a zero intercept on the volume adsorbed axis. On the other hand, if the surface has some fraction of strong sites, offering a higher heat of physical adsorption than the remainder of the surface, the linear portion of the isotherm will show a positive intercept on the volume adsorbed axis. This intercept will represent the volume of gas adsorbed on strong sites[77]. Griffiths *et al.* measured isotherms for very low pressure N_2 physical adsorption at −196°C on Graphon previously reacted in O_2 to different levels of burn-off[78]. The sample gasified to 20% burn-off had ~12.5 m^2/g of its total surface existing as strong (presumably edge) sites. It is interesting that this area is considerably larger than those estimated from oxygen chemisorption[72,73] and somewhat larger than the area occupied by oxygen complex following gasification of V3G to 20% burn-off at 550°C in 2×10^4 Pa of O_2, as found by Taylor[73]. Taylor's rate data for V3G, normalized using both the 300°C chemisorption data and the physical adsorption data, are shown in Fig. 9.

More recently Ranish, in this laboratory, measured the reactivity of SP-1 graphite in various pressures of O_2 ranging from 0.1 to 5.1 MPa[79]. As discussed previously[80], SP-1 graphite is a highly purified, ground natural graphite which has a mean particle diameter of ~30 μm and a thickness of ~0.5 μm. The ASA of the graphite burned off to 20% at 577°C in O_2 was estimated, from oxygen chemisorption in 0.1 MPa O_2 at 300°C, to be 0.13 m^2/g. The Thomy and Duval technique[81], employing physical adsorption of Kr at −196°C, was used to estimate the basal plane area. From the height of the first step in the isotherm compared to the height of the step for exfoliated graphite (assumed to have 100% basal plane area), the basal plane area was estimated to be 1.6 m^2/g out of a total area of 3.6 m^2/g for the 20% burned off sample. Again, the ASA estimated from physical adsorption is much higher than that estimated from oxygen chemisorption, in the absence of carbon gasification, at 300°C.

Figure 15 summarizes the reactivity results of Ranish conducted at pressures ranging from 0.1–3.5 MPa

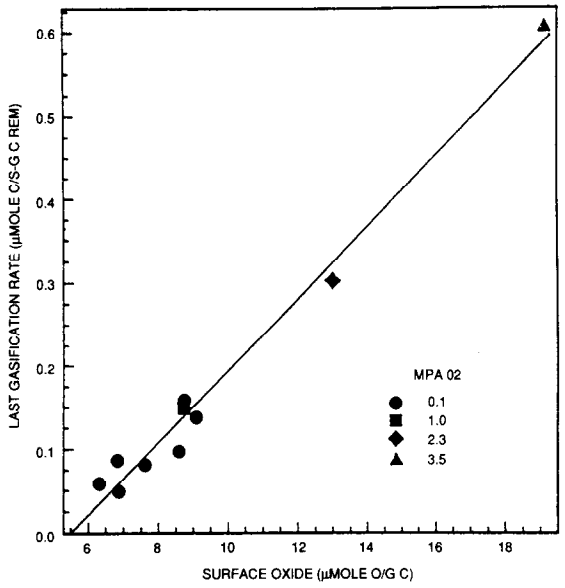

Fig. 15. Relationship between gasification rate of SP-1 graphite at 577°C and 20% burn-off and amount of surface oxide recovered following shut down[79].

O_2 and a temperature of ~577°C to 20% burn-off. Shown are the last gasification rates versus the surface oxide existing on the surface at the completion of the runs. The oxide remaining on the surface is estimated to occupy a surface area increasing from 0.37 to 0.94 m^2/g as reactant pressure increases from 0.1 to 3.5 MPa. These values are considerably in excess of the area occupied by complex following a chemisorption experiment at 300°C but less than the total high energy site area estimated from physical adsorption. Specific reaction rates, normalized on the basis of ASA estimated from oxygen chemisorption at 300°C and Kr physical adsorption at −196°C, are included in Fig. 9. From a least squares calculation, the best straight line through the data points in Fig. 9 gives an activation energy of 255 kJ/mole.

In summary, a reasonably coherent picture for the kinetics of the C-O_2 reaction has emerged. The importance of active sites to the reaction has been shown by a number of workers to be unmistakable. In the case of carbons where microscopy or the "ruler" cannot be used to measure rates of recession at active sites, there is yet some uncertainty as to how to quantitatively measure active site concentration in order to determine specific reaction rates.

3.2 *Rate constants for hydrocarbon CVD reactions*

Just as active sites are important in determining specific gasification rates of carbons in oxidizing gases, they should also be important in determining rates at which hydrocarbons crack over active carbon sites to deposit additional carbon. We set out to confirm this importance by following the rate of propylene cracking and subsequent carbon deposition over Graphon samples which were burned off in O_2 at 450°C to different levels[82–84]. Following burn-off, the samples were outgassed at 950°C to remove oxygen complex from the ASA prior to studying rates of propylene cracking. The rate of propylene disappearance and product formation was followed in a static reactor using a mass spectrometer. The starting propylene pressure (1.5 Pa) was kept low to assure that gas phase cracking of proplyene was insignificant. This was true at reaction temperatures between 600–800°C.

Propylene cracks over a carbon surface to yield almost entirely H_2, methane, ethylene, and surface carbon and hydrogen. Following an induction period, the rate of cracking is first order in propylene pressure. Further, the rate of carbon deposition is proportional to the rate of propylene cracking. The rate of propylene disappearance can be given as

$$\frac{-d(C_3H_6)}{dt} = k\,(\text{area})(C_3H_6). \qquad (6)$$

If the area is assumed to be the TSA, as determined by N_2 physical adsorption at −196°C and the BET equation, values of k could be calculated for Graphon samples having different levels of burn-off. Results are summarized on the Arrhenius plot, Fig. 16. As expected, TSAs do not normalize the rate data. Rather, calculated values of k increase with the extent of burn-off which the Graphon has undergone.

At this point it was of interest to consider how to measure a meaningful ASA for carbons whose surfaces are catalyzing the decomposition of propylene. The obvious question was, does propylene chemi-

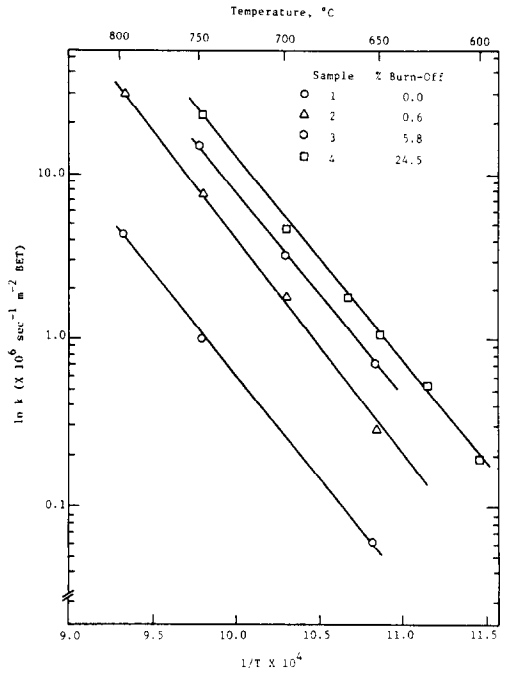

Fig. 16. Arrhenius plots of rate constant for propylene cracking over Graphon samples of different burn-off, normalized to TSA[83].

sorb on carbon active sites and could such chemisorption be used to normalize propylene CVD rate data? It was surprising to us that even though there are voluminous results published on the physical adsorption of hydrocarbons on carbon surfaces[85], results on chemisorption are essentially nonexistent. Using an approach similar to our oxygen chemisorption studies, we selected a chemisorption temperature considerably below the temperature where propylene cracking occurred at a measurable rate, that is 300°C. Adsorption was rapid, with equilibrium occurring within 15 min. To determine whether chemisorption of propylene could be measured, two adsorption runs were made, with outgassing at 300°C between the two runs. The first adsorption run would measure the total of physical and chemical (if there were any) adsorption. Outgassing between runs would remove only the physically adsorbed propylene from the carbon surface. The second run would then measure just physical uptake of propylene, with the difference between the two uptakes representing chemisorbed propylene. Chemisorption of propylene could be measured at 300°C, yielding a Langmuir isotherm with uptake being constant at pressures >0.6 Pa.

The ASAs occupied by chemisorbed propylene on the various Graphon samples were calculated assuming a molecular area for the molecule of 0.234 nm^2[86]. ASA's increased from 0.056 m^2/g for the original Graphon to 1.9 m^2/g for the sample burned off in O_2 to a weight loss of 24.5%. Now rate constants were calculated by substituting ASA's in equation (6). Results, summarized on an Arrhenius plot in Fig. 17, show that meaningful rate constants can now be obtained. Note that the units of the rate constant are now cm/s. These units are produced by multiplying the units ($1/cm^2 \cdot s$) by the reactor volume used. Thus, the rate constant is normalized for general use if the ASA is known. The best line through the data gives an activation energy of 238 kJ/mole for the cracking of propylene over carbon active sites. Since the rate of carbon deposition is proportional to the rate of propylene disappearance, meaningful rate constants can also be obtained for carbon deposition[83], the data again giving an activation energy of 238 kJ/mole.

Literally billions of dollars have been spent learning how to produce pyrolytic carbons from hydrocarbon CVD, having different morphologies and properties. Uses of pyrolytic carbons have ranged from heart valves[87], to nose cones in rockets[88], to coatings for nuclear fuel particles[89]. Surprisingly, though, relatively little funds have been spent to support attempts to understand the fundamentals of the CVD process. Clearly, this understanding must include considerations of the importance of ASA. Much research is yet to be done.

4. CARBON MOLECULAR SIEVES

As discussed by Walker *et al.*[90], carbon molecular sieves (CMS) contain a large specific pore volume primarily in pores of molecular dimensions. Potential energy diagrams can be calculated for molecules interacting with the basal plane surface of a carbon crystallite using the sum of a Lennard–Jones potential for the dispersive and repulsive energies[90]. As a molecule approaches the basal plane sufficiently closely from a large distance, the dispersive energy of attraction is at first significant and predominant, leading to a potential energy minimum, corresponding to physical adsorption at some equilibrium distance from the surface. This distance is about $2^{1/6}\sigma$, where σ is the kinetic diameter of the molecule. As the molecule approaches the surface more closely than this equilibrium distance for physical adsorption, the repulsive potential energy quickly becomes predominant, leading to the requirement of an activation energy for this closer approach. As a consequence, an activation energy will also be required for a molecule to diffuse through a pore if the surfaces of the pore are sufficiently close together. This is known as activated diffusion. The ability to sieve, or separate, different molecules rests upon the fact that small differences in molecular size or pore size produce large differences in the activation energy required for diffusion in the repulsive region of a potential energy diagram. Table 8 presents calculated critical pore dimensions for a number of gases, assuming that the pore is slit shaped with its sides composed of carbon basal planes. For slit widths smaller than the sizes given, the molecule (gas) will undergo activated diffusion, where the dif-

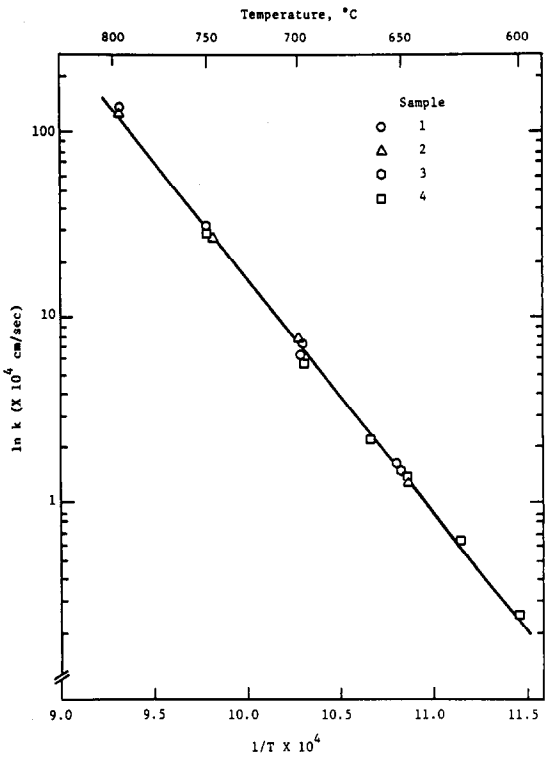

Fig. 17. Arrhenius plots of rate constants for propylene cracking over Graphon samples of different burn-off, normalized to ASA[83].

Table 8. Summary of calculated critical pore dimensions[91]

Gas	Slit width (nm)
CO	0.541
H_2	0.548
CO_2	0.542
O_2	0.544
N_2	0.572
Ar	0.575
He	0.508

fusion coefficient varies exponentially with absolute temperature. For slit widths somewhat larger than the sizes given, the molecule will undergo Knudsen diffusion, where the diffusion coefficient varies with $T^{0.5}$.

Carbon molecular sieves are produced from organic precursors which either do not pass through a fluid range upon their carbonization (so-called thermosetting precursors) or, if they do pass through a fluid range, lead to nonplanar free radical intermediates. Chars, as opposed to cokes, are produced which contain small, cross-linked, poorly aligned, trigonally bonded crystallites. The result is a crude aperture-cavity material, where the cavities supply a high internal surface area connected by apertures of molecular dimensions.

It would appear that some of the earliest workers to appreciate the potential of producing CMS were Dacey and Thomas[92,93]. They used as a precursor polyvinylidene chloride $(C_2H_2Cl_2)_n$. Upon its carbonization, HCl is liberated leaving a porous char behind. They found that flat molecules, like benzene, could be taken up by the char much more rapidly than branched molecules like neopentane. They thus concluded that the apertures in their CMS were slit-shaped. They were successful in separating mixtures of neopentane and either *n*-pentane or benzene. They appear to be among the first workers to have also recognized the potential of altering the aperture size in a CMS by adsorbing a hydrocarbon on it[93]. Following adsorption, the hydrocarbon was pyrolyzed, depositing carbon within the pore system.

In this laboratory, we continued to examine the production of CMS from polyvinylidene chloride (PVDC)[94]. We showed that maximum heat treatment temperature (HTT) plays a critical role in determining the size of the apertures in CMS. Figure 18, for example, shows the effect of HTT on the surface areas of PVDC carbons calculated from uptake of four molecules of different minimum dimensions over a 1 h period. At low HTT, HCl has not been completely released from the structure and thus the aperture opening is partially blocked. Over the HTT range from ~600 to 1000°C, the aperture size is at a maximum; and little sieving is seen between

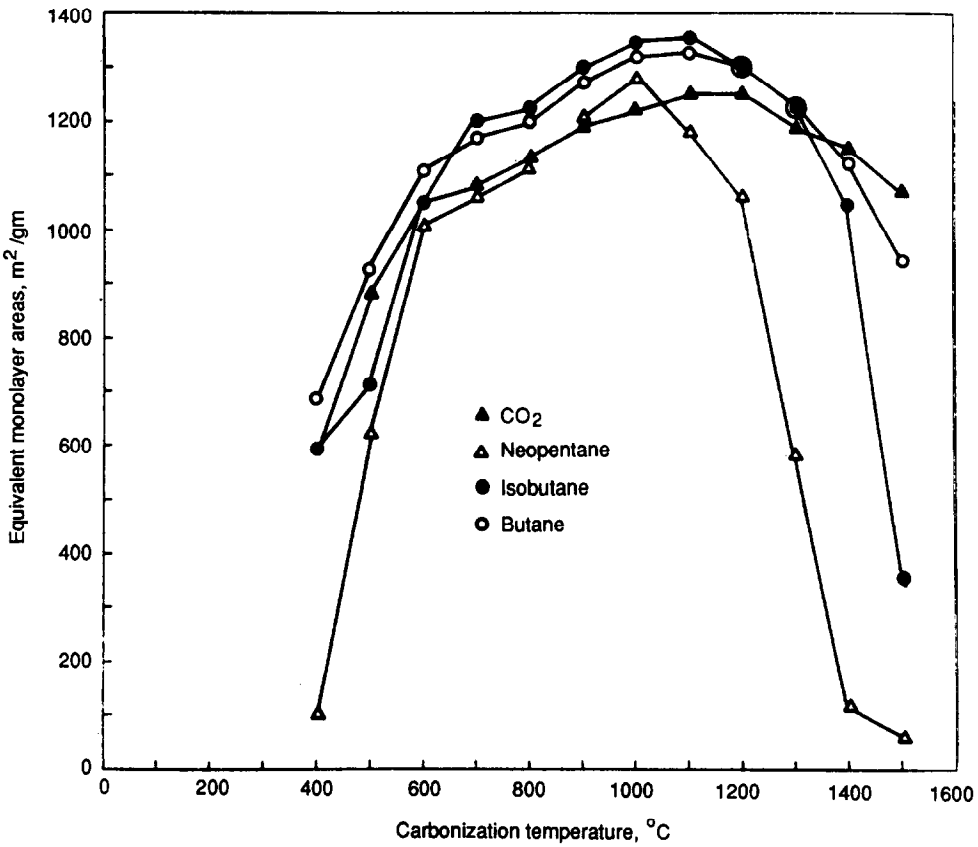

Fig. 18. Surface areas of polyvinylidene chloride carbons heated to different temperatures[94].

the smallest molecule CO_2 (minimum cross-section of ~0.33 nm) and neopentane (minimum cross-section of ~0.62 nm). Heat treatment to higher temperatures results in the breakage of some cross-links in the structure, its densification, and a gradual reduction in aperture size—thus creating a molecular sieve. If one heats to a sufficiently high temperature, the apertures are closed to all gases, including He. A large surface area will still exist in the cavities, however, as determined from SAXS studies.

We later showed the potential of using a CMS produced from Saran (a copolymer of PVDC and polyvinyl chloride) to separate a branched from a straight chain hydrocarbon in a flow system[95]. Pellets were produced from Saran char (filler) and lignite pitch (binder). The behavior of the CMS is compared with those of two microporous materials, a 5A zeolite from Linde and a BPL activated carbon from Calgon Corporation (Fig. 19). The zeolite, which is used commercially to separate hydrocarbons, shows the expected performance on a break through plot. The branched hydrocarbon,2,2,4-trimethylpentane, has negligible access to the pores within the zeolite; it breaks through the bed almost immediately. The straight chain hydrocarbon, *n*-heptane, rapidly diffuses through the apertures within the zeolite and adsorbs in the cavities; thus it exhibits a considerable hold-up time before breaking through the bed. Pores in the activated carbon are sufficiently large that it exhibits essentially the same break through time for both hydrocarbons. The CMS exhibit excellent sieving behavior for the hydrocarbons; the break through time for the branched hydrocarbon is short and that for the straight chain hydrocarbon is even longer than that found for a comparable weight of the zeolite.

As expected, once the potential of producing CMS from PVDC was demonstrated, there was a rush to look for a number of other possible precursors including synthetic polymers and naturally occurring thermosetting materials like selected coals and cellulose[96–104]. The early interest was primarily in utilizing CMS for the separation of hydrocarbons. To the author's knowledge, the only commercial use today in this area is in chromatography[105]. More recently, there has been interest and commercial utilization of CMS for the separation of N_2 and O_2 in air[102]. As seen in Table 8, O_2 can enter slightly smaller slits than N_2 without encountering activated diffusion. Using unsteady state diffusion measurements we obtained diffusion coefficients for some important gases in a CMS produced from a non-coking bituminous coal[106]. Results are summarized on an Arrhenius plot, Fig. 20, and Table 9. The diffusion parameter (D/r_0^2) in units of $1/s$ is plotted instead of the diffusion coefficient (D), since the average diffusion length (r_0) within a particle of CMS is unknown. Orders of magnitude difference exist between the diffusion parameter for O_2 and N_2. As found previously[107], N_2 and Ar have essentially identical diffusion coefficients. In disagreement with results of theoretical calculations shown in Table 8,

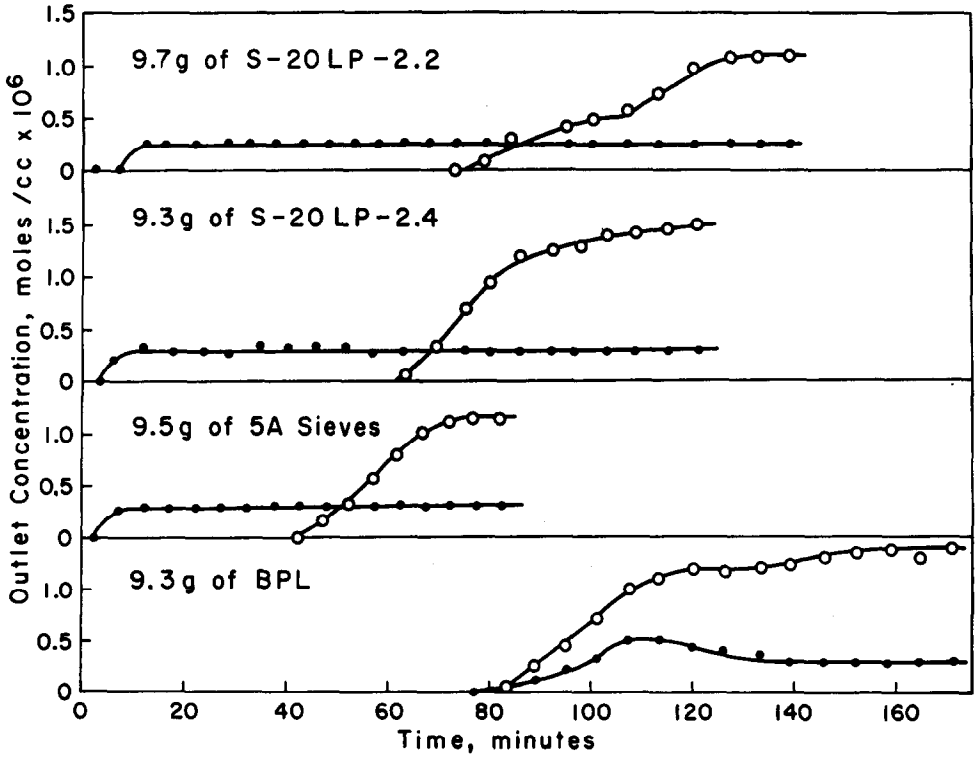

Fig. 19. Breakthrough plots for *n*-heptane (○) and 2,2,4-trimethylpentane (●) over microporous solids[95].

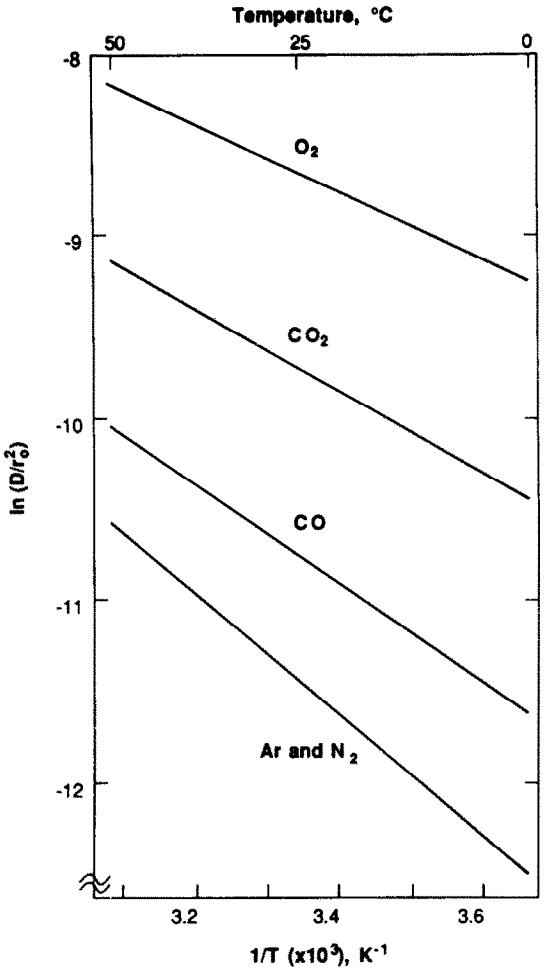

Fig. 20. Arrhenius plots of diffusion parameters for gases diffusing through a CMS[106].

the activation energy for O_2 diffusion is smaller than those for diffusion of CO_2 and CO. Koresh and Soffer also find that uptake of CO in their CMS is slower than that found for O_2[108,109]. However, they find that uptake of CO_2 is more rapid than that of O_2, in contrast to our studies. It could be that results are affected by what species is chemisorbed on the ASA of the CMS. The CMS used in our studies, for example, was passivated by exposure to H_2 at 150°C and 5.4 MPa pressure. As a result, hydrogen was chemisorbed, preventing the subsequent chemisorption of oxygen. This could affect the interaction energy between a diffusing species and a surface and, thus, the exact shape of the potential energy diagram.

Table 9. Activation energies for gases diffusing in a CMS

Gas	Activation energy (kJ/mole)
O_2	14
CO_2	19
CO	23
N_2	30
Ar	30

In recent years, there has been great interest in using zeolite molecular sieves as catalysts for shape selective reactions[110]. Concurrent with this activity, we were interested in using CMS as catalyst supports for shape-selective reactions[111–114]. Metals in the form of organometallics, metallic acids, or salts can be added to the organic precursor (monomer) prior to its polymerization and carbonization. A system examined by Schmitt and Walker[111,112] was furfuryl alcohol and chloroplatinic acid. Prior to complete polymerization, this mixture was added to an activated carbon, which upon polymerization and carbonization to 700°C resulted in the formation of macrocracks within the composite. The macrocracks served as rapid diffusion pathways to the molecular sized pores. The final sample was a CMS containing 1% Pt by weight, exhibiting separation between straight chain and branch chain hydrocarbons. Selective hydrogenation of a straight and branch chain olefin in essentially 0.1 MPa flowing H_2 was measured at 150°C, using a bed of this catalyst. Results are summarized in Fig. 21. The straight chain olefin, 1-butene, is effectively hydrogenated to *n*-butane. Negligible hydrogenation or isomerization of 3-methyl-1-butene occurs, since the branched molecule has little access to the Pt catalyst within the pores of the CMS.

5. CONCLUSIONS

Following completion of my Sigma Xi lecture in 1961, I said "Progress in the development of new carbon materials and in the improvement of old carbon materials will continue to be recorded—as a chapter in the over-all story of materials science." Following completion of my Skakel lecture in 1971, I said, in part, "The new materials science of carbon and graphite (from benzene to graphite) will be developed; and, as a consequence, much more interest and recognition will be seen in universities in this field. Indeed, the new materials science of organic materials will take its place along side of the fields

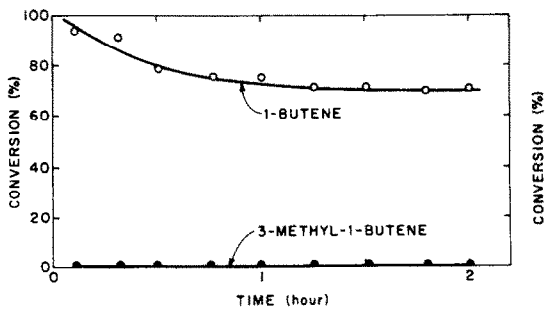

Fig. 21. Competitive hydrogenation of 1-butene and 3-methyl-1-butene over CMS-Pt catalyst at 150°C. Residence time, 1.8 s[112].

of metallurgy and ceramic science as an important area."

Since 1961, we have seen tremendous advances in carbon science. In part, this is because university faculties expanded their interests in carbon science, as I predicted. This expansion of their interest will continue as carbon exhibits potential for still more applications in new areas.

Acknowledgments—I particularly want to recognize the financial support which our carbon research program at Penn State received from Federal and State agencies and industry over the many years. I am most grateful. I also recognize the many pleasures I have derived from my interactions with colleagues working in carbon science throughout the world. This is a wonderfully, close-knit group conducting their studies of carbon through a truly interdisciplinary approach.

REFERENCES

1. P. L. Walker, Jr., *Am. Scientist* **50**, 259 (1962).
2. P. L. Walker, Jr., *Carbon* **10**, 369 (1972).
3. P. L. Walker, Jr., J. F. Rakszawski, and G. R. Imperial, *J. Phys. Chem.* **63**, 140 (1959).
4. P. L. Walker, Jr., F. Rusinko, Jr., and L. G. Austin, In *Advances in Catalysis* (Edited by D. D. Eley, P. W. Selwood, and P. B. Weisz), Vol. 11, pp. 133–221. Academic Press, New York (1959).
5. S. D. Cameron and D. J. Dwyer, *Langmuir* **4**, 282 (1988).
6. M. Audier and M. Coulon, *Carbon* **23**, 317 (1985).
7. M. Endo, *Chemtech* **18**, 568 (1988).
8. W. R. Ruston, M. Warzee, J. Hennaut, and J. Waty, *Carbon* **7**, 47 (1969).
9. P. A. Tesner, E. V. Robinovich, I. S. Rafalkes, and E. F. Arefieva, *Carbon* **8**, 435 (1970).
10. R. T. K. Baker, P. S. Harris, R. B. Thomas, and R. J. Waite, *J. Catal.* **30**, 86 (1973).
11. M. Audier, M. Coulon, and A. Oberlin, *Carbon* **18**, 73 (1980).
12. M. Audier, A. Oberlin, M. Oberlin, M. Coulon, and L. Bonnetain, *Carbon* **19**, 217 (1981).
13. M. Audier, J. Guinot, M. Coulon, and L. Bonnetain, *Carbon* **19**, 99 (1981).
14. P. L. Walker, Jr., J. F. Rakszawski, and G. R. Imperial, *J. Phys. Chem.* **63**, 133 (1959).
15. R. E. Franklin, *Acta Cryst.* **4**, 253 (1951).
16. J. S. Speck, M. Endo, and M. S. Dresselhaus, J. Crystal Growth, **94**, 834 (1989).
17. A. Oberlin, *Carbon* **22**, 521 (1984).
18. R. Phillips, F. J. Vastola, and P. L. Walker, Jr., Proceedings Third Industrial Carbon and Graphite Conference, London, p. 257 (1971).
19. J. D. Brooks and G. H. Taylor, *Carbon* **3**, 185 (1965).
20. J. D. Brooks and G. H. Taylor, In *Chemistry and Physics of Carbon* (Edited by P. L. Walker, Jr.), Vol. 4, pp. 243–286. Dekker, New York (1968).
21. C. R. Kinney, R. C. Nunn, and P. L. Walker, Jr., *Ind. Eng. Chem.* **49**, 880 (1957).
22. J. J. Madison and R. M. Roberts, *Ind. Eng. Chem.* **50**, 237 (1958).
23. I. C. Lewis and T. Edstrom, *J. Org. Chem.* **28**, 2050 (1963).
24. A. Marchand and J. V. Zanchetta, *Carbon* **3**, 483 (1966).
25. P. L. Walker, Jr. and A. Weinstein, *Carbon* **5**, 13 (1967).
26. A. Weintraub, M. S. Thesis, The Pennsylvania State University, 1967.
27. T. Edstrom and I. C. Lewis, *Carbon* **7**, 85 (1969).
28. A. Weintraub and P. L. Walker, Jr., Proceedings Third Industrial Carbon and Graphite Conference, London, p. 75 (1971).
29. H. Marsh, F. Dachille, J. Melvin, and P. L. Walker, Jr., *Carbon* **9**, 159 (1971).
30. E. Fitzer, K. Mueller, and W. Schaefer, In *Chemistry and Physics of Carbon* (Edited by P. L. Walker, Jr.) Vol. 7, pp. 237–383. Dekker, New York (1971).
31. H. Marsh, J. M. Foster, G. Hermon, M. Iley, and J. N. Melvin, *Fuel* **52**, 243 (1973).
32. P. W. Whang, F. Dachille, and P. L. Walker, Jr., *High Temperature-High Pressure* **6**, 127 (1974).
33. I. C. Lewis, Division Polymer Chemistry Reprints, American Chemical Society **14**, No. 1, 380 (1973).
34. I. C. Lewis, *Carbon* **18**, 191 (1980).
35. A. W. Scaroni, Ph.D. Thesis, The Pennsylvania State University (1981).
36. I. C. Lewis, *Carbon* **20**, 519 (1982).
37. T. M. Peters, M. S. Thesis, The Pennsylvania State University (1982).
38. R. R. Griffin, P. L. Walker, Jr. and A. W. Scaroni, Abstracts Sixteenth Biennial Conference on Carbon, p. 16 (1983).
39. R. A. Greinke and I. C. Lewis, *Carbon* **22**, 305 (1984).
40. R. R. Griffin, M. S. Thesis, The Pennsylvania State University (1984).
41. S. E. Stein, *Carbon* **19**, 421 (1981).
42. B. Pullman, Proceedings Third Biennial Conference on Carbon, Pergamon Press, Oxford, p. 3 (1959).
43. M. Zander, *Fuel* **65**, 1019 (1986).
44. C. A. Coulson and A. Streitwieser, Jr., *Dictionary of Pi-Electron Calculations*. W. H. Freeman and Company, San Francisco (1965).
45. M. D. Tilicheev, *J. Appl. Chem.* (U.S.S.R.) **12**, 741 (1939).
46. I. Mochida, T. Oyama, Y. Korai, and Y. Q. Fei, *Fuel* **67**, 1171 (1988).
47. J. L. White and R. J. Price, *Carbon* **12**, 321 (1974).
48. S. Eser, G. G. Karsner, and F. J. Derbyshire, Abstracts Eighteenth Biennial Conference on Carbon, p. 52 (1987).
49. J. Abrahamson, *Carbon* **11**, 337 (1973).
50. G. R. Hennig, In *Chemistry and Physics of Carbon* (Edited by P. L. Walker, Jr.), Vol. 2, pp. 1–49. Dekker, New York (1966).
51. J. J. Baker, Ph.D. Thesis, The Pennsylvania State University, 1970.
52. E. L. Evans and J. M. Thomas, Proceedings Third Industrial Carbon and Graphite Conference, London, p. 3 (1971).
53. R. T. Yang and C. Wong, *J. Chem. Phys.* **75**, 4471 (1981).
54. R. T. K. Baker and P. S. Harris, *Carbon* **11**, 25 (1973).
55. R. T. K. Baker and J. J. Chludzinski, *Carbon* **19**, 75 (1981).
56. J. M. Thomas, In *Chemistry and Physics of Carbon* (Edited by P. L. Walker, Jr.), Vol. 1, pp. 121–202. Dekker, New York (1965).
57. E. L. Evans, R. J. M. Griffiths, and J. M. Thomas, *Science* **171**, 174 (1971).
58. A. W. Moore, In *Chemistry and Physics of Carbon* (Edited by P. L. Walker, Jr. and P. A. Thrower), Vol. 11, pp. 69–187. Dekker, New York (1973).
59. G. S. Rellick, P. A. Thrower, and P. L. Walker, Jr., *Carbon* **13**, 71 (1975).
60. F. Rodriquez-Reinoso and P. L. Walker, Jr., *Carbon* **13**, 7 (1975).
61. R. C. Bansal, F. J. Vastola, and P. L. Walker, Jr., *J. Colloid Interface Sci.* **32**, 187 (1970).
62. R. N. Smith, D. A. Young, and R. A. Smith, *Trans. Faraday Soc.* **62**, 2280 (1966).
63. J. J. Lander and J. Morrison, *J. Appl. Phys.* **35**, 3593 (1964).

64. M. Barber, E. L. Evans, and J. M. Thomas, *Chem. Phys. Letters* **18**, 423 (1973).
65. P. J. Hart, Ph.D. Thesis, The Pennsylvania State University, 1966.
66. R. Phillips, F. J. Vastola, and P. L. Walker, Jr., *Carbon* **8**, 197 (1970).
67. R. C. Bansal, F. J. Vastola, and P. L. Walker, Jr., *Carbon* **8**, 443 (1970).
68. G. Tremblay, F. J. Vastola, and P. L. Walker, Jr., *Carbon* **16**, 35 (1978).
69. R. Lussow, Ph.D. Thesis, The Pennsylvania State University, 1966.
70. E. A. Kmetko, Proceedings First and Second Carbon Conference, U. Buffalo, p. 21 (1956).
71. W. R. Smith and M. H. Polley, *J. Phys. Chem.* **60**, 689 (1956).
72. N. R. Laine, F. J. Vastola, and P. L. Walker, Jr., *J. Phys. Chem.* **67**, 2030 (1963).
73. R. L.Taylor, Ph.D., The Pennsylvania State University, 1982.
74. B. McCarroll and D. W. McKee, *Carbon* **9**, 301 (1971).
75. A. J. Bennett, B. McCarroll, and R. P. Messmer, *Phys. Rev. B* **3**, 1397 (1971).
76. M. R. Hayns, *Theoret. Chim. Acta(Berl.)* **39**, 61 (1975).
77. D. Graham, *J. Phys. Chem.* **61**, 49 (1957).
78. D. W. L. Griffiths, W. J. Thomas, and P. L. Walker, Jr., *Carbon* **1**, 515 (1964).
79. J. M. Ranish, Ph.D. Thesis, The Pennsylvania State University, 1984.
80. P. L. Walker, Jr., L. G. Austin, and J. J. Tietjen, In *Chemistry and Physics of Carbon* (Edited by P. L. Walker, Jr.), Vol. 1, pp. 327–365. Dekker, New York (1965).
81. A Thomy, and X. Duval, *J. Chim. Phys.* **66**, 1966 (1969).
82. W. P. Hoffman, F. J. Vastola, and P. L. Walker, Jr., *Carbon* **22**, 585 (1984).
83. W. P. Hoffman, F. J. Vastola, and P. L. Walker, Jr., *Carbon* **23**, 151 (1985).
84. W. P. Hoffman, F. J. Vastola, and P. L. Walker, Jr., *Carbon* **26**, 485 (1988).
85. N. N. Avgul and A. V. Kiselev, In *Chemistry and Physics of Carbon* (Edited by P. L. Walker, Jr.), Vol. 6, pp. 1–124. Dekker, New York (1970).
86. W. P. Hoffman, Ph.D. Thesis, The Pennsylvania State University (1979).
87. J. C. Bokros, L. D. LaGrange, and F. J. Schoen, In *Chemistry and Physics of Carbon* (Edited by P. L. Walker, Jr. and P. A. Thrower), Vol. 9, pp. 103–171. Dekker, New York (1973).
88. W. V. Kotlensky, In *Chemistry and Physics of Carbon* (Edited by P. L. Walker, Jr. and P. A. Thrower), Vol. 9, pp. 173–262. Dekker, New York (1973).
89. M. R. Everett, D. V. Kinsey, and E. Romberg, In *Chemistry and Physics of Carbon* (Edited by P. L. Walker, Jr.), Vol. 3, pp. 289–436. Dekker, New York (1968).
90. P. L. Walker, Jr., L. G. Austin, and S. P. Nandi, In *Chemistry and Physics of Carbon* (Edited by P. L. Walker, Jr.), Vol. 2, pp. 257–371. Dekker, New York (1966).
91. M. R. Rao, R. G. Jenkins, and W. A. Steele, *Langmuir* **1**, 137 (1985).
92. J. R. Dacey and D. G. Thomas, *Trans. Faraday Soc.* **50**, 740 (1954).
93. J. R. Dacey and D. G. Thomas, *Can. J. Chem.* **33**, 244 (1955).
94. T. G. Lamond, J. E. Metcalfe, III, and P. L. Walker, Jr., *Carbon* **3**, 59 (1965).
95. P. L. Walker, Jr., Mineral Industries, The Pennsylvania State University, January, 1966, pp. 1–7.
96. J. J. Kipling and R. B. Wilson, *Trans. Faraday Soc.* **56**, 557 (1960).
97. J. J. Kipling and R. B. Wilson, *Trans. Faraday Soc.* **56**, 562 (1960).
98. J. J. Kipling, J. Sherwood, P. V. Shooter, and N. R. Thompson, *Carbon* **1**, 321 (1964).
99. P. L. Walker, Jr., T. G. Lamond, and J. E. Metcalfe, III, Proceedings Second Industrial Carbon and Graphite Conference, London, p. 7 (1966).
100. S. P. Nandi and P. L. Walker, Jr., *Fuel* **54**, 169 (1975).
101. S. P. Nandi and P. L. Walker, Jr., *Separation Sci.* **11**, 441 (1976).
102. H. Juntgen, K. Knoblauch, and K. Harder, *Fuel* **60**, 817 (1981).
103. J. E. Metcalfe, III, M. Kawahata, and P. L. Walker, Jr., *Fuel* **42**, 233 (1963).
104. R. L. Patel, S. P. Nandi, and P. L. Walker, Jr., *Fuel* **51**, 47 (1972).
105. R. Kaiser, *Chromatographia* **3**, 38 (1970).
106. Y. Nakayama, S. K. Verma, and P. L. Walker, Jr., Unpublished results (1984).
107. K. Chihara, M. Suzuki, and K. Kawazoe, *J. Colloid Interface Sci.* **64**, 584 (1978).
108. J. Koresh and A. Soffer, *J.C.S. Faraday I* **76**, 2457 (1980).
109. J. Koresh and A. Soffer, *J.C.S. Faraday I* **76**, 2472 (1980).
110. J. M. Thomas, *Angew. Chem. Int. Ed. Engl.* **27**, 1673 (1988).
111. J. L. Schmitt, Jr. and P. L. Walker, Jr., *Carbon* **9**, 791 (1971).
112. J. L. Schmitt, Jr. and P. L. Walker, Jr., *Carbon* **10**, 87 (1972).
113. P. L. Walker, Jr., A. Oya, and O. P. Mahajan, *Carbon* **18**, 377 (1980).
114. C. Moreno-Castilla, O. P. Mahajan, P. L. Walker, Jr., H.-J. Jung, and M. A. Vannice, *Carbon* **18**, 271 (1980).